A fast tool for the parametric analysis of human body exposed to LF electromagnetic fields in biomedical applications

A Fast Tool for the Parametric Analysis of Human Body Exposed to LF Electromagnetic Fields in Biomedical Applications

Riccardo Torchio[a,*], Alessandro Arduino[b], Luca Zilberti[b], Oriano Bottauscio[b]

[a]*Department of Industrial Engineering, Università degli Studi di Padova, 35131 Padova, Italy*
[b]*Istituto Nazionale di Ricerca Metrologica, 10135 Torino, Italy*

Abstract

A numerical procedure for analyzing electromagnetic (EM) fields interactions with biological tissues is presented. The proposed approach aims at drastically reducing the computational burden required by the repeated solution of large scale problems involving the interaction of the human body with EM fields, such as in the study of the time evolution of EM fields, uncertainty quantification, and inverse problems. The proposed volume integral equation (VIE), focused on low frequency applications, is a system of integral equations in terms of current density and scalar potential in the biological tissues excited by EM fields and/or electrodes connected to the human body. The proposed formulation requires the voxelization of the human body and takes advantage of the regularity of such discretization by speeding-up the computational procedure. Moreover, it exploits recent advancements in the solution of VIE by means of iterative preconditioned solvers and *ad hoc* parametric Model Order Reduction techniques. The efficiency of the proposed tool is demonstrated by applying it to a couple of realistic model problems: the evaluation of the peripheral nerve stimulation due to the gradient coils of a magnetic resonance imaging scanner during a clinical examination and the assessment of the exposure to environmental fields at 50 Hz of live-line workers with uncertain properties of the biological tissues. Thanks to the proposed method, uncertainty quantification analyses and time domain simulations are possible even for large scale problems and they can be performed on standard computers and reasonable computation time. Sample implementation of the method is made publicly available at `https://github.com/UniPD-DII-ETCOMP/BioMOR`.

Keywords: Bio-electromagnetism, computational electromagnetics, electromagnetic (EM) analysis fast methods, integral equations, magnetic resonance imaging (MRI), Peripheral Nerve Stimulation (PNS), Uncertainty Quantification

1. Introduction

The computation of the electromagnetic (EM) fields generated within the human body by an external source, which can be a system of coils [1] or a system of electrodes [2], is required by different

*Corresponding author: riccardo.torchio@unipd.it (R. Torchio)

biomedical applications. For instance, Maxwell's equations must be solved in the human body when evaluating the exposure to the EM fields produced by a magnetic resonance imaging (MRI) scanner [1, 3, 4]; when planning an oncological hyperthermia treatment driven by magnetic fields [5]; when studying Transcranial Magnetic Stimulation (TMS) for the treatment of neurodegenerative diseases [6, 7]; or, when assessing the exposure to environmental EM fields [8, 9, 10, 11, 12, 13, 14, 15].

The recent evolution of the computing resources allowed for handling large scale EM problems, whose computational domain includes the entire human body, in reasonable computation times (of the order of hours [16]), although with a significant requirement in terms of memory (about 50 GB for 1 million degrees of freedom [17], depending on the type of problem and adopted method). However, some advanced applications require the repeated solution of such large scale problem multiple times, for different values of few input parameters. This happens, for example, in the study of the time evolution of EM fields described in the frequency domain in presence of the skin effect, like in high conductive materials [18]. Another case which requires the repeated solution of such large scale EM problems is in uncertainty quantification (UQ), where, generally, the Monte Carlo (MC) method is used to quantify the uncertainty of some quantities of interest arising from the randomness, or the lack of knowledge, of some input parameters [19, 20]. A third case where repeated solutions of the EM problem are required is in inverse problems [21], like the optimal design of dielectric pads for shimming in high-field MRI [22] or the quantitative imaging of the electric properties from MRI measurements [23, 24].

Despite the possibility of handling large scale problems for some direct evaluations, when the number of required repeated solutions grows significantly, the global computational cost of the advanced applications becomes unaffordable, making the entire problem unsolvable from a practical point of view. In order to deal with this kind of computationally demanding large scale problems, parametric Model Order Reduction (pMOR) approaches can be adopted [25]. The number of degrees of freedom of the original problem (of the order of some millions for an entire human body) is significantly reduced by pMOR, which limits the problem complexity while substantially keeping the accuracy of the original solver. Thus, whereas the solution of the single original problem requires some hours of computation, the solution of the reduced model is almost instantaneous; therefore, repeated solutions of the problem varying some parameters can be performed in a reasonable time.

The objective of this paper is twofold. On the one hand, an Integral Equations (IE) method formulation [16, 26, 27, 28] of the low frequency (LF) EM problem is presented. This formulation is numerically convenient for evaluating the exposure of the human body to the EM fields. Indeed, anatomical models of the human body are usually provided with a voxel-based discretization [29, 30] (cf. Fig. 1), originating directly from MRI scans or other tomographic acquisitions. The proposed formulation takes advantage of the regularity of this discretization by reducing the memory requirement and speeding-up the computational procedure. Moreover, it exploits recent advancements in

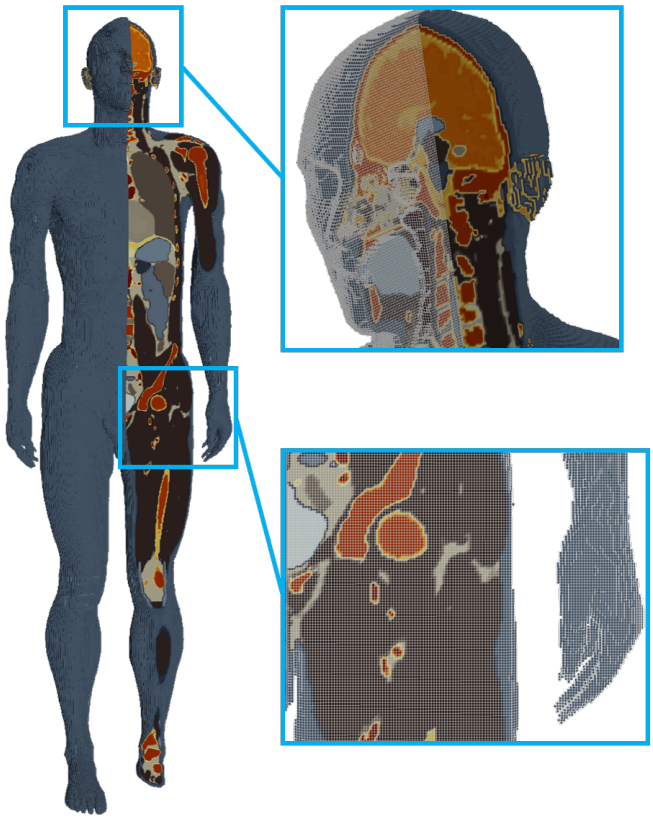

Figure 1: Voxel-based anatomical human model Duke from the Virtual Population [30] discretized with a mesh of 2 mm. Each color identifies a different biological tissue.

the solution of IE by means of iterative preconditioned solvers [31, 32].

On the other hand, two *ad hoc* pMOR schemes are presented. One dealing with problems in which the frequency of the EM radiation is a varying parameter, the other one for problems in which the resistivity of the biological tissues is affected by uncertainty. Despite of the different nature of the selected parameters, both can take advantage of the adoption of a pMOR scheme, which significantly reduces the computational complexity of the analysis of human body exposure to the EM fields, opening to the possibility of performing it on desktop computers.

The proposed formulation and the pMOR schemes are applied to a couple of realistic model problems: the evaluation of the peripheral nerve stimulation (PNS) due to the gradient coils (GCs) of an MRI scanner during a clinical examination (the signals have a frequency range up to some tens of kilohertz); and the assessment of the exposure to environmental fields at 50 Hz of live-line workers with uncertain properties of the biological tissues. In the first problem, a modified version of the anatomical human model Yoon-Sun from the Virtual Population with a hip, a knee, and a shoulder implant is considered. In this application, the solution of many problems at different frequencies is

imposed by the skin effect that takes place in the metallic implants at the considered frequencies. On the other hand, the human model Duke from the Virtual Population (cf. Fig. 1) is used for the second problem, in which the MC method is applied to the pMOR scheme in order to estimate the probability distribution of the peak of the induced electric field. In both cases, the models are discretized with a 2 mm mesh, thus resulting in large scale computational problems (about $6.8{\cdot}10^6$ voxels in the first case and $8.4{\cdot}10^6$).

The adopted formulation and its numerical modelling are presented in Section 2, whereas the pMOR schemes are introduced in Section 3. Finally, in Section 4, the presented numerical methods are applied to the realistic model problems and the results are discussed.

2. Numerical Method

In this section, the theoretical background of the proposed numerical method is described by taking as example the human body model introduced in the previous section. First, in Section 2.1, the formulation is shortly described. Then, in Section 2.2, the discretization procedure is performed according to [33, 31, 32] in order to exploit the translational invariant property of the integral kernel, drastically speeding-up the simulation and dramatically reducing the memory requirement. Then, in Section 2.3, a solution technique based on an Algebraic Multigrid (AMG) preconditioner is presented, leading to a significant reduction of the overall computational cost required by human-body EM simulations [32, 34].

2.1. Formulation

First, the following well-known equation, where all field quantities are assumed to be phasors, is introduced [35]:

$$\mathbf{E}(\mathbf{r}) = -i\omega\mathbf{A}(\mathbf{r}) - \nabla\varphi(\mathbf{r}) + \mathbf{E}_{ext}(\mathbf{r}), \tag{1}$$

where $\mathbf{E}$ is the electric field, $\mathbf{A}$ is the magnetic vector potential, and φ is the scalar electric potential. $\mathbf{E}_{ext}$ is the incident external field produced by the unperturbed source, $\mathbf{r}$ is the position, i is the imaginary unit, and ω is the angular frequency. The forcing term $\mathbf{E}_{ext}$ is proportional to the magnetic vector potential of the source, $\mathbf{A}_{ext}$, as highlighted in the following Section 3.1. Vector potential in (1) is given by its integral expression, i.e.

$$\mathbf{A}(\mathbf{r}) = \mu_0 \int_\Omega \mathbf{J}(\mathbf{r}')g(\mathbf{r},\mathbf{r}')d\Omega, \tag{2}$$

where $\mathbf{J}$ is the conduction current density vector, $\mathbf{r}'$ is the integration point, and $g(\mathbf{r},\mathbf{r}')$ is the Green's function of vacuum [36, 35]. Ohm's law relation is then introduced:

$$\mathbf{E}(\mathbf{r}) = \rho(\mathbf{r})\mathbf{J}(\mathbf{r}), \text{ with } \mathbf{r} \in \Omega, \tag{3}$$

where ρ is the electric resistivity.

Coupling (1) with (3), one obtains the equation where $\mathbf{J}$ and φ are the problem unknowns and $\mathbf{A}$ depends on $\mathbf{J}$ through (2):

$$\rho(\mathbf{r})\mathbf{J}(\mathbf{r}) + i\omega\mathbf{A}(\mathbf{r}) + \nabla\varphi(\mathbf{r}) = \mathbf{E}_{ext}(\mathbf{r}). \tag{4}$$

For the sake of simplicity, since we are focusing on low/medium frequency applications, the conduction current density is considered divergence free, thus (4) is complemented by

$$\nabla \cdot \mathbf{J} = 0. \tag{5}$$

Equations (1)–(5) must now be discretized. In this work, with the aim of exploiting the translational invariant property of Green's function, the conductive domain (i.e. the human body) is discretized by means of a structured mesh consisting of regular hexahedral elements (i.e. voxels). Indeed, when the human model is obtained starting from the segmentation of a tomography, it is usually directly provided in a voxel-based format.

Then, the current density vector is expanded by using vector shape functions related to the internal faces of the mesh (N_f), i.e.

$$\mathbf{J}(\mathbf{r}) = \sum_{k=1}^{N_f} \mathbf{w}_k(\mathbf{r}) j_k, \tag{6}$$

where $\mathbf{w}_k$ is the kth vector shape function and j_k is the flux of $\mathbf{J}$ through the kth internal face of the mesh. Unknowns j_k, with $k = 1, \cdots, N_f$, are stored in the array $\mathbf{j}$. The electric scalar potential is also expanded as in [37] by using piece-wise constant basis functions. Therefore, the array $\mathbf{\Phi}$ of size N_v (where N_v is the number of human-body voxels) is also introduced, which stores the unknowns related to φ.

By using (6) and exploiting the Galerkin scheme, the continuum equations (1)–(5) are discretized and the following system of equations is obtained:

$$\begin{bmatrix} \mathbf{R} + i\omega\mathbf{L} & \mathbf{G} \\ \mathbf{G}^T & \mathbf{0} \end{bmatrix} \begin{bmatrix} \mathbf{j} \\ \mathbf{\Phi} \end{bmatrix} = \begin{bmatrix} \mathbf{e_{ext}} \\ \mathbf{j_{ext}} \end{bmatrix}, \tag{7}$$

where $\mathbf{R}$ and $\mathbf{L}$ are the (sparse) resistance and (dense) inductance matrices, respectively, whose coefficients are given in [32]. In (7), $\mathbf{G}$ is the volumes–faces incidence matrix whereas $\mathbf{e_{ext}}$ is the array corresponding to the incident external electric field, and $\mathbf{j_{ext}}$ is the array corresponding to injected currents (which can be used to model human model connections to electrodes injecting positive or negative currents). For the sake of clarity, it is worth noting that the problem described by (7) can be seen as a fully coupled electric circuit with a very large number of components and where voxels are the circuit nodes, while the internal faces of the mesh (which connect two voxels) are the circuit branches [35]. Thus, $\mathbf{G}$ is the incidence matrix of the equivalent circuit.

System (7) can be theoretically solved by means of direct or preconditioned–iterative solvers. However, as previously discussed in Section 1, the size of the problem (i.e. the number of unknowns)

is typically very large for human body models (several millions of unknowns), making the computational cost of the problem possibly prohibitive, both in terms of computation time and memory requirement. This is mostly due to matrix $\mathbf{L}$, which is dense and its storage has a $\mathcal{O}(N_f^2)$ complexity. Thus, the following sections show how to exploit the regularity of the mesh in order to drastically reduce the computational cost required for the solution of (7).

2.2. Data-Sparse Representation of Matrix $\mathbf{L}$

One of the major computational bottlenecks in solving (7) is the memory required for the storage of the dense matrix $\mathbf{L}$, which grows quadratically with the number of unknowns [26]. However, thanks to its dependence on Green's function, matrix $\mathbf{L}$ has a hierarchical off-diagonal low-rank (HODLR) structure, which can be exploited by using data-sparse approximation techniques as done by many works in the literature where, e.g., Hierarchical Matrices coupled with cross approximation [38, 39, 26], Fast Multiple Method [40], or other techniques [41] are used. These approaches are powerful computational tools which, in general, may allow for extremely reducing the computational cost required for the storage of $\mathbf{L}$ and they also speed-up algebraic operations. However, these approaches are in general intrusive and mostly based on matrix compression (therefore introducing unavoidable, hopefully small, approximations), which usually requires some expertise from the user who *a priori* has to choose suitable values for the compression tolerances [42, 26, 38].

In this work, since a regular mesh consisting of all equal voxels is used, matrix $\mathbf{L}$ possesses further useful mathematical properties which can be exploited. Namely, as discussed in [42], matrix $\mathbf{L}$ can be embedded into a Block Toeplitz matrix with Toeplitz Blocks (BTTB); then, such BTTB matrix can be represented by means of a circulant tensor which, roughly, allows reducing the memory requirement to $\mathcal{O}(N)$ and the matrix-vector products to $\mathcal{O}(Nlog(N))$ by using the Fast Fourier Transform (FFT) and its inverse (IFFT) [27]. This numerical approach allows for drastically reducing the computational burden due to the dense matrix $\mathbf{L}$ and, contrary to other methods, it does not introduce any approximation since no data-compression is applied and therefore mutual EM interactions are exactly considered.

By using such an approach, the computational issues due to the full matrix $\mathbf{L}$ are solved. However, since the system of equations (7) has a large dimension and matrix $\mathbf{L}$ has been replaced by a mathematical operator, an efficient iterative solver must be used. Such a solver must not require to explicitly store system (7); instead it must exploit an equivalent mathematical operator which performs matrix-vector products such as GMRES.

To this aim, it is of fundamental importance to adopt a proper preconditioner to reduce the number of required iterations. In this regard, the following section presents an efficient preconditioner which allows for further reducing the computational cost required by solving (7).

2.3. Algebraic Multigrid Preconditioner

As previously discussed, solving (7) by means of an iterative solver like GMRES may require a prohibitive number of iterations if no preconditioning is adopted. In [31], where a similar system of equations is considered, a preconditioner is constructed by replacing the matrix block (1,1) of (7) with its diagonal and by exploiting the Schur complement technique. This preconditioning approach is very efficient (i.e., a limited number of iterations are required by GMRES to reach the convergence). However, when the Schur complement is performed at each preconditioned–GMRES iteration, the following system of equations must be solved:

$$\{\mathbf{G}^T[diag(\mathbf{R}+i\omega\mathbf{L})]^{-1}\mathbf{G}\}\mathbf{a}=\mathbf{b}, \tag{8}$$

where $\mathbf{a}$ and $\mathbf{b}$ are arrays of size equal to the number of voxels.

Since $\mathbf{G}$ is very sparse and the inverse of the diagonal of $\mathbf{R}+i\omega\mathbf{L}$ is used, the resulting system (8) is also very sparse. However, as already discussed, the number of voxels in the human body model can be very large (several millions), therefore solving (8) can be computationally demanding if a direct solver is used. Fortunately, the structure of (8) is very similar to the one resulting from finite difference methods and therefore it can be efficiently solved by means of an Algebraic MultiGrid (AMG) solver [43, 34]. One of the main advantage of AMG is that it requires a reduced memory since it does not require to factorize the whole system matrix. Moreover, solving (8) by means of AMG requires two subsequent steps, i.e., 1) a pre-processing of the system matrix is performed in order to construct the hierarchical multigrid levels and, 2) the system is solved by exploiting such AMG levels and the hierarchical representation of (8). Since, in the proposed method, AMG is used as preconditioner for solving (7), system (8) must be solved several times (as many as the number of iterations required by GMRES to converge) for different $\mathbf{b}$ but the left-hand-side is always the same. Therefore, the construction of the multigrid levels (step 1) can be performed only once and then, at each GMRES iteration, system (8) is solved by exploiting the same multigrid construction, therefore significantly reducing the overall computational cost.

3. (Parametric) Model Order Reduction

In the section above, some numerical strategies have been proposed in order to efficiently solve a single large scale problem (7). However, in several applications [18, 20, 22, 23, 24], (7) must be solved several times for several frequency values or by varying the resistivity of human-body tissues and organs. All these modifications affect the terms in the matrix of (7). For instance, if time-domain analyses must be performed, the FFT and IFFT can be used in order to move the problem from time to frequency and then from frequency to time; thus, several frequency domain simulations must be performed. Another case of interest is when UQ or sensitivity analyses are performed, and therefore

several simulations with different resistivity distributions are required in the context of, e.g., a MC simulation.

Although the computational cost required to solve the single problem (7) has been significantly reduced thanks to the techniques presented in the previous section, solving (7) several times can be computationally demanding since hundreds or even tens of thousands simulations are typically required when time domain simulations or UQ are preformed [44].

To solve this problem, pMOR techniques can be exploited in order to construct an equivalent parametric Reduced Order Model (pROM) of (7), whose solution can be performed very efficiently with a reduced memory requirement and very short computation time [45, 46].

In the following sections, a MOR algorithm based on Proper Orthogonal Decomposition (POD) [47], and which exploits the solution strategy techniques presented in Section 2.2, is presented. First, the case of frequency sweep simulations is considered, therefore having the frequency as parameter (which is required when, e.g., time-domain analyses are performed). Then, the case of parametric resistivity is considered, which is of interest when UQ with random material properties is required.

3.1. Transient/Frequency Analyses

The starting point to create an EM pROM of the human body having the frequency as parameter is (7). However, before proceeding, it is useful to represent the external field as

$$\mathbf{E}_{ext}(\mathbf{r}) = -i\omega\mathbf{A}_{ext}(\mathbf{r}), \tag{9}$$

where $\mathbf{A}_{ext}$ is the incident (external) magnetic vector potential generated by the source coil system (e.g., the GCs system of an MRI scanner). Thus, in order to make the frequency dependence explicit, it is useful to represent (7) as

$$\begin{bmatrix} \mathbf{R} + i\omega\mathbf{L} & \mathbf{G} \\ \mathbf{G}^T & \mathbf{0} \end{bmatrix} \begin{bmatrix} \mathbf{j} \\ \mathbf{\Phi} \end{bmatrix} = \begin{bmatrix} -i\omega\mathbf{a_{ext}} \\ \mathbf{j_{ext}} \end{bmatrix}, \tag{10}$$

where $\mathbf{a_{ext}}$ is the array corresponding to $\mathbf{A}_{ext}$.

The aim is to find an equivalent pROM of (10) in a frequency range of interest, i.e. $f \in [f_{min}, f_{max}]$. To do that, the iterative procedure reported in Algorithm 1 is used. Basically, such procedure selects some characteristic values of the frequency in the range $f \in [f_{min}, f_{max}]$, solves the problem for such frequency values and uses the corresponding solution to project the full order problem into a reduced base.

Thus, according to Algorithm 1, the first frequency value for which (10) is solved is selected as the central value of the frequency range of interest, i.e. $f = \frac{f_{min}+f_{max}}{2}$. Then, the desired tolerance value, η, for the accuracy of the pROM with respect to the right-hand-side of (10) is also selected. Such value is typically chosen as $\eta = 10^{-4}$.

Algorithm 1 pMOR Algorithm

Input: Matrices $\mathbf{G}$ and $\mathbf{R}$. Matrix $\mathbf{L}$ represented by the equivalent circulant tensor. Arrays $\mathbf{a_{ext}}$ and $\mathbf{j_{ext}}$. The frequency range for the pROM, i.e. $f = [f_{min}, f_{max}]$

Set $\omega = 2\pi \frac{f_{min}+f_{max}}{2}$ // 0

Set $res_\star = +\infty$

Set N_{rand} (e.g. $N_{rand} = 20$)

Set a desired value of η (e.g. $\eta = 10^{-4}$)

while $res_\star > \eta$ **do**

Find the solution $\mathbf{x}$ of (10) // 1

Update the orthonormal basis // 2

Generate/Update the reduced order model // 3

Generate N_{rand} random values of $f \in [f_{min}, f_{max}]$ // 4

for $h = 1, \cdots, N_{rand}$ **do**

Select the hth random frequency

Find the solution $\hat{\mathbf{x}}$ of the reduced order problem // 5

Evaluate the residual, res, with respect the full order problem // 6

end for

Find the frequency value ($f_\star$) generated at step 4 which maximizes the residual and assign the corresponding maximum residual to $res_\star$. The new angular frequency used for the next iteration is $\omega = 2\pi f_\star$ // 7

end while

Output: Reduced order model and the projection matrix

Then, at step 1 of Algorithm 1, the full order problem (10) is solved for $\omega = 2\pi f$ and the solution $\mathbf{x} = \left[\mathbf{j}, \mathbf{\Phi}\right]^T$, is obtained by using the techniques described in Section 2.2 and Section 2.3.

At step 2 of Algorithm 1, using the solution $\mathbf{x}$ found at the previous step, the projection matrix $\mathbf{V}$ is generated/updated by applying a Gram-Schmidt Orthogonalization (GSO), i.e.,

$$\mathbf{V} = \mathrm{GSO}([\mathbf{V}, \mathbf{x}]). \tag{11}$$

It is worth noting that the equation above should be intended in an algorithmic sense, i.e. the new projection matrix $\mathbf{V}$ (left-hand-side of (11)) is updated by adding to the old $\mathbf{V}$ (right-hand-side of (11)) a new column (i.e. $\mathbf{x}$) and applying the GSO to the resulting matrix. At iteration one of the Algorithm, since $\mathbf{V}$ has not been created yet, $\mathbf{V}$ at the right-hand-side of (11) is obviously taken as the empty matrix.

Then, at step 3 of Algorithm 1, an attempt of the pROM is obtained by using the projection matrix found at the previous step, i.e.

$$\hat{\mathbf{R}} = \mathbf{V}^* \begin{bmatrix} \mathbf{R} & \mathbf{G} \\ \mathbf{G}^T & \mathbf{0} \end{bmatrix} \mathbf{V}, \qquad \hat{\mathbf{L}} = \mathbf{V}^* \begin{bmatrix} \mathbf{L} & \mathbf{0} \\ \mathbf{0} & \mathbf{0} \end{bmatrix} \mathbf{V}, \tag{12}$$

$$\hat{\mathbf{a}}_{\mathbf{ext}} = \mathbf{V}^* \begin{bmatrix} \mathbf{a_{ext}} \\ \mathbf{0} \end{bmatrix}, \qquad \hat{\mathbf{j}}_{\mathbf{ext}} = \mathbf{V}^* \begin{bmatrix} \mathbf{0} \\ \mathbf{j_{ext}} \end{bmatrix}, \tag{13}$$

where $\hat{\mathbf{R}}$ and $\hat{\mathbf{L}}$ are the reduced order matrices and $\hat{\mathbf{a}}_{\mathbf{ext}}$ and $\hat{\mathbf{j}}_{\mathbf{ext}}$ are the reduced order right-hand-side arrays. Symbol $*$ indicates the conjugate transpose. It is worth noting that, at each iteration, the size of the reduced matrices and arrays increases by one since the number of columns of $\mathbf{V}$ has increased by one at step 2 of the algorithm.

In (12), a matrix-matrix product involving the dense matrix $\mathbf{L}$ is required. However, such product can be efficiently performed by exploiting the equivalent circulant tensor of $\mathbf{L}$, thus it is not required to actually store and generate the full matrix $\mathbf{L}$ (which would otherwise require a prohibitive computational cost for its storage and for the algebraic operations).

After having created the provisional pROM, its accuracy must be tested. Therefore, at step 4 of Algorithm 1, N_{rand} frequencies in the range $[f_{min}, f_{max}]$ are selected (with, e.g., $N_{rand} = 20$). Then, at step 5 of Algorithm 1, the provisional pROM is used to solve the problem for each random frequency, i.e.,

$$\hat{\mathbf{x}} = [\hat{\mathbf{R}} + i\omega\hat{\mathbf{L}}] \backslash [\hat{\mathbf{j}}_{\mathbf{ext}} - i\omega\hat{\mathbf{a}}_{\mathbf{ext}}] \tag{14}$$

where $\hat{\mathbf{x}}$ is the solution of the pROM. Then, the approximate solution of the full order model, $\tilde{\mathbf{x}}$, is obtained by using $\mathbf{V}$:

$$\tilde{\mathbf{x}} = \mathbf{V}\hat{\mathbf{x}}, \tag{15}$$

which means that $\tilde{\mathbf{x}}$ is obtained as a linear combination of the other solutions found at step 1 of Algorithm 1.

At step 6 of Algorithm 1, the corresponding residual, res, is evaluated, i.e.,

$$res = \left\| \begin{bmatrix} \mathbf{R} + i\omega\mathbf{L} & \mathbf{G} \\ \mathbf{G}^T & \mathbf{0} \end{bmatrix} [\tilde{\mathbf{x}}] - \begin{bmatrix} -i\omega\mathbf{a}_{\mathbf{ext}} \\ \mathbf{j}_{\mathbf{ext}} \end{bmatrix} \right\|. \tag{16}$$

Finally, at step 7 of Algorithm 1, the maximum residual, $res_\star$, and the corresponding frequency $f_\star$ are selected. If $res_\star$ is greater than the prescribed tolerance η, then a new iteration of the algorithm is performed by selecting $\omega = 2\pi f_\star$. Instead, if $res_\star < \eta$, the algorithm stops and the pROM is created.

It is worth noting that the pMOR algorithm requires the solution the full order model, i.e. (10), as many times as the number of iterations required by Algorithm 1 to converge. However, as shown in the Results section, for the target problem of this paper a limited number of iterations is generally required (in the order of tens). Then, the pMOR can be used to solve the frequency domain problem for a generic frequency in the range $[f_{min}, f_{max}]$ with a truly negligible computational cost. Thus, frequency-sweep simulations with tens of thousands (or even more) frequency values can be solved very efficiently with a limited overall computational cost, i.e. the one required to generate the pROM. Indeed, the dimension of the pROM is equal to the number of iterations required by Algorithm 1 to reach the convergence (generally in the order of tens) and the solution of pMOR (i.e., (14)) is therefore very fast (less than one second).

3.2. Uncertainty Quantification

In the previous section the frequency has been chosen as parameter of the problem. Instead, in this section, the resistivity of the biological tissues are considered as the parameters of the problem (for each biological tissue a resistivity value is assigned). For each biological tissue, an independent parameter is considered. Therefore, in this case we have N_p parameters, where N_p is the number of biological tissue where the resistivity is considered as a varying quantity. Namely, $\rho_k \in [\rho_{k,min}, \rho_{k,max}]$, with $k = 1, \cdots, N_p$, are the problem parameters (equivalently, the conductivity can be considered in place of the resistivity). Thus, in this case, the starting parametric problem is still (7), where the resistance matrix is now given by

$$\mathbf{R} = \mathbf{R}_0 + \sum_{k=1}^{N_p} \rho_k \mathbf{R}_k, \tag{17}$$

where $\mathbf{R}_0$ is the resistance matrix related to the biological tissues where the resistivity is considered as a fixed quantity (the resistivity is assigned to its nominal value in each biological tissue where such parameter is considered fixed, i.e. a non-varying quantity, and zero elsewhere), whereas $\mathbf{R}_k$ is the (unitary) resistance matrix related to the kth domain (i.e., the resistivity is taken equal to 1 in the kth domain and zero elsewhere).

Then, the pROM can be constructed by using a procedure equivalent to the one reported in the previous section where the frequency was considered as varying parameter.

Therefore, a pROM is iteratively constructed as in (12)–(13), with the difference that several reduced resistance matrices are obtained, i.e.,

$$\hat{\mathbf{R}}_0 = \mathbf{V}^* \begin{bmatrix} \mathbf{R}_0 & \mathbf{G} \\ \mathbf{G}^T & \mathbf{0} \end{bmatrix} \mathbf{V}, \qquad \hat{\mathbf{R}}_k = \mathbf{V}^* \begin{bmatrix} \mathbf{R}_k & \mathbf{0} \\ \mathbf{0} & \mathbf{0} \end{bmatrix} \mathbf{V}, \tag{18}$$

with $k = 1, \cdots, Np$, and the solution of the pROM is obtained as

$$\hat{\mathbf{x}} = [\hat{\mathbf{R}}_0 + \sum_{k=1}^{N_p} \rho_k \hat{\mathbf{R}}_k + i\omega\hat{\mathbf{L}}] \backslash [\hat{\mathbf{j}}_{\mathbf{ext}} - i\omega\hat{\mathbf{a}}_{\mathbf{ext}}]. \tag{19}$$

With the above considerations, it is possible to construct a pMOR of the problem having the resistivity of several tissues as varying parameters. However, a numerical issue concerning the stop criterion for construction of the pROM must be discussed.

Indeed, unfortunately, unknowns $\mathbf{j}$ and $\mathbf{\Phi}$ vary in a very different way with the variation of the resistivity parameters. This fact leads to a large number of iterations required by pMOR to converge and, possibly, the resulting pROM can be ill-conditioned. To solve this numerical problem, one should note that finding the scalar electric potential, i.e. $\mathbf{\Phi}$, is not actually important in practice since the total electric field in any point of the space only depends on $\mathbf{j}$.

Having in mind this considerations, a different stop criterion which only tests the accuracy of the current array $\mathbf{j}$ obtained from the pMOR can be adopted. Thus, the main idea is to replace (16)

with the following

$$res = \left\| \begin{bmatrix} \mathbf{C}^T & \mathbf{0} \\ \mathbf{0} & \mathbf{1} \end{bmatrix} \left(\begin{bmatrix} \mathbf{R} + i\omega\mathbf{L} & \mathbf{G} \\ \mathbf{G}^T & \mathbf{0} \end{bmatrix} [\tilde{\mathbf{x}}] - \begin{bmatrix} -i\omega\mathbf{a_{ext}} \\ \mathbf{j_{ext}} \end{bmatrix} \right) \right\|, \tag{20}$$

where, with respect to (16), a matrix operator has been applied to the left. Such a matrix operator is made by the curl faces–edges incidence matrix $\mathbf{C}$, which is the algebraic equivalent of the curl operator and satisfies the following property

$$\mathbf{C}^T\mathbf{G} = \mathbf{0}. \tag{21}$$

Therefore, as desired, the effect of $\mathbf{\Phi}$ on res is eliminated. To give a physical interpretation, by applying the matrix operator $\mathbf{C}$, the residual (20) checks the accuracy of the pMOR by evaluating the time derivative of the incident magnetic field, i.e. $i\omega\mathbf{C}^T\mathbf{a}_{ext}$.

By following the above discussion, the number of iterations required by the pMOR algorithm to converge, and therefore also the size of the pROM, is significantly reduced and the resulting model is well-conditioned.

4. Results

In this section, the proposed numerical approach is applied to two realistic problems:

1. the evaluation of the PNS due to the low-frequency magnetic field generated by the GCs of an MRI scanner during a clinical examination;
2. the assessment of the exposure to environmental fields of live-line workers with uncertain resistivity of the biological tissues.

In the first case, a time-domain problem is solved by superposing the results at different frequencies in order to follow the trend of the electric field induced within the biological tissues of the patient; therefore, the MOR scheme proposed in Section 3.1 is used. The peak of the induced electric field in each voxel is the dosimetric quantity to be compared with the guidelines in this application. Instead, for the second case, the MOR scheme proposed in Section 3.2 is used, since the lack of knowledge on the resistivity of the biological tissues suggests their modelling as random variables. The dosimetric quantity of this problem is the maximum of the electric field magnitude, conveniently filtered in order to remove possible numerical outliers [8]. Since some input parameters are modelled as random variables, the output of the problem is a random variable as well, estimated through the MC method applied to the pROM. Sample MATLAB implementation of the method is made publicly available at `https://github.com/UniPD-DII-ETCOMP/BioMOR`.

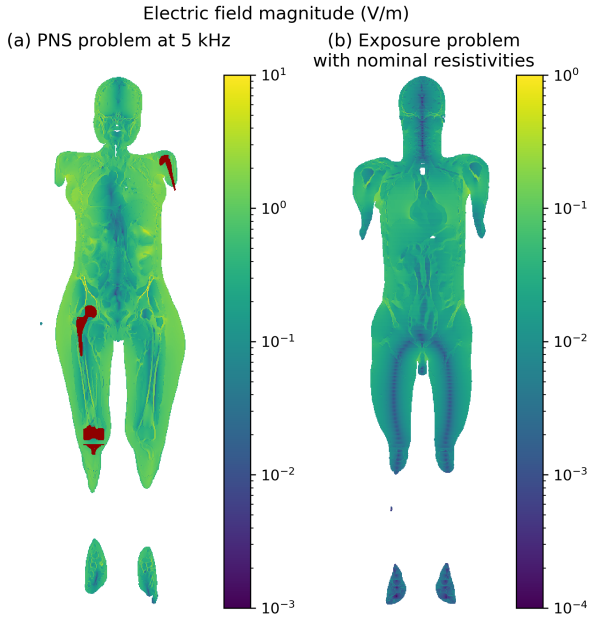

Figure 2: Magnitude of the electric field distributions computed by solving the complete problems for a given selection of the parameters. On the left (a), the solution to the PNS problem in presence of orthopaedical implants at the frequency of 5 kHz; on the right (b), the solution to the exposure problem with nominal resistivities.

4.1. PNS due to the GCs of an MRI scanner

The switched magnetic field generated by the GCs of an MRI scanner can induced PNS in the patient [48]. Thus, the eddy currents induced within the biological tissues must be monitored by means of numerical simulations. In the specific case of patients with metallic orthopaedic implants, the distribution of the eddy currents in the biological tissues could be altered by the more relevant eddy currents induced within the metallic parts of the implant.

In order to assess the induction of PNS in implanted patients, the anatomical human model Yoon-Sun from the Virtual Population has been modified through a virtual surgery to include a hip, a knee, and a shoulder implant. Since the three implants are sufficiently distant from each other to not cause EM interactions, a single model with all the three implants is simulated here. The magnitude of the electric field induced in the model by a uniform harmonic magnetic field of 1 mT at the frequency 5 kHz with direction perpendicular to the transversal plane is shown in Fig. 2a.

Since the GCs are supplied according to particular pulse sequences, in order to assess the induction of PNS the time evolution of the induced electric field must be taken into account. Instead of solving the EM problem in the time-domain, the time evolution can be monitored by solving the problem at different frequencies and then combining the results.

The GCs supply waveforms contain harmonics up to some tens of kilohertz, which fall in a linearity range for the low conductive biological tissues, but are high enough to induce the skin

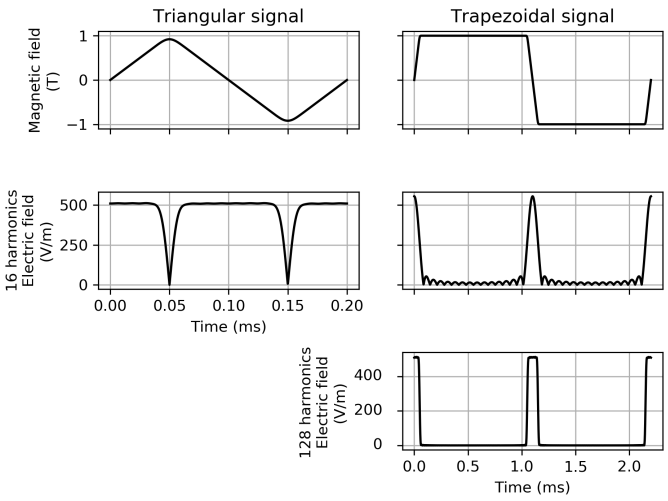

Figure 3: Waveforms of: first row, the magnetic field produced by the GCs; second row, the electric field recovered with 16 harmonics; third row, the electric field recovered with 128 harmonics. The first column is about a triangular supply, whereas the second one is about a trapezoidal supply.

effect in the metallic implants. Thus, the computation of the time evolution can take advantage of the pROM for frequency sweep described in Section 3.1.

The considered model discretized by a structured mesh with $2\,\text{mm} \times 2\,\text{mm} \times 2\,\text{mm}$ voxels has a computational domain of about $6.8 \cdot 10^6$ voxels, which leads to about $27{\cdot}10^6$ degrees of freedom (DoF). A complete simulation of this problem at a certain frequency with the proposed numerical formulation requires about 30 minutes on a machine with 2 processors Intel Xeon CPU E5-2680 v2 @ 2.80 GHz and 128 GB of RAM.

As can be seen from the estimated trends reported in Fig. 3 for the electric field in a voxel of tissue near the hip implant, the number of frequencies required to recover the time evolution depends on the supplied waveform. It can vary from 16 harmonics for the triangular signal up to 128 harmonics for the trapezoidal signal. Since each harmonic requires a complete simulation, by using the full order model (FOM), 144 simulations of about 30 minutes each are needed to recover the two trends reported in Fig. 3.

On the other hand, the described MOR scheme in the range $[1\,\text{Hz}, 100\,\text{kHz}]$ with a tolerance $\eta = 10^{-4}$ leads to a pROM with only 15 DoFs, whose computations requires the solution of just 15 complete problems. The successive solution of the pROM is almost instantaneous, so the computational time needed to estimate the time evolution of the electric field is less than one-hundredth the times needed using the FOM. Moreover, with a negligible computational cost, other realistic pulse sequences can be simulated. Quantitative details about the FOM and the pROM for the PNS problem are collected in Table 1.

Table 1: Computational data for a single solution (PNS case).

	DoFs	Time (s)	Memory (GB)
FOM	$\sim 27 \cdot 10^6$	~ 1800	~ 8.5
pROM	15	$\ll 1$	$\ll 1$

Table 2: Computational data for a single solution (UQ case).

	DoFs	Time (s)	Memory (GB)
FOM	$\sim 33 \cdot 10^6$	~ 2200	~ 10.4
pROM	173	$\ll 1$	$\ll 1$

4.2. UQ for the Human Body Exposure to Environmental Fields

In this case, the assessment of the exposure to environmental EM fields of live-line workers with uncertain properties of the biological tissues is considered. In particular, the exposure to the magnetic field generated by a 380 kV overhead line at 50 Hz when the line is close to the chest of the worker is analysed (cf. case A.2 investigated in [9]).

The human body model considered in this case consists of about $8.4{\cdot}10^6$ voxels, leading to about $24{\cdot}10^6$ internal faces. The generation of the dense matrix $\mathbf{L}$ would require a prohibitive memory, i.e. about 1500 TB. Instead, by following the approach of Section 2.2, only about 5 GB are required to store the circulant tensor corresponding to matrix $\mathbf{L}$. As previously discussed, the MOR scheme proposed in Section 3.2 has been adopted by setting the desired tolerance η equal to 10^{-4}. In this analysis, the resistivity of the 30 biological tissues which exhibit the highest electric field in a simulation performed with the nominal value of the parameters have been considered as 30 independent parameters, with resistivity varying in the range $\pm 20\%$ with respect to the nominal value. Such MOR scheme has required 173 iterations, therefore leading to a pROM of size 173.

Table 2 shows the computational data required for the solution of the FOM and the pROM. As can be seen, the computational complexity required by the pROM is drastically reduced with respect to the one required by the FOM.

Thus, thanks to the pROM, a UQ analysis by means of MC has been possible. Such an analysis has been repeated by considering 5, 10, 20, and 30 random resistivities varying with a uniform probability distribution in the range $\pm 20\%$ with respect their nominal value. The four MC simulations have been performed with 10000 evaluations. It is worth noting that using the FOM in MC would have required 255 days (i.e., $2200{\times}10000$ s), thus leading to a prohibitive computation time. Instead, by using the pROM, the MC simulation has required only some hours.

The magnitude of the electric field distribution computed with the nominal resistivities can be found in Fig. 2b. The results of the UQ analysis for 5, 10, and 20 parameters are reported in Fig. 4

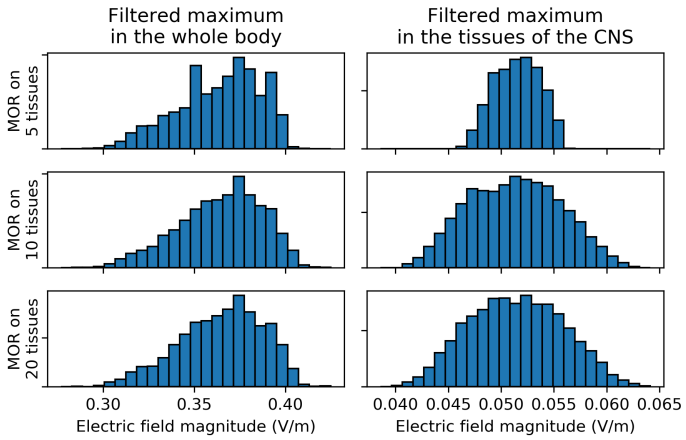

Figure 4: Relative frequency histograms of the maximum electric field magnitude in the whole body (first column) and in the central nervous system (CNS, second column), estimated by the filter described in [8]. The histograms are produced by a MC method applied on the pROM obtained by MOR executed on 5 tissues (first row), 10 tissues (second row) and 20 tissues (third row). The resistivity of the selected tissues is varied in the range $\pm 20\%$ with respect to their nominal value.

in terms of the probability density function of the maximum electric field magnitude in the whole body and in the central nervous system (CNS), estimated by the filter described in [8]. As can be seen, the results obtained by considering 10 and 20 parameters are very similar, and the same consideration holds for 30 parameters, although they are not reported for the sake of conciseness. On the other hand, the results provided by the pROM constructed on top of just 5 parameters leads to a significantly different uncertainty propagation, especially for the peak in the CNS.

In summary, the overall analysis has required 173 solutions of the FOM (to construct the pROM) and then 10 000 solutions of the pROM for the MC analysis.

5. Conclusions

An *ad hoc* computational method is proposed to reduce the computational complexity arising from the repeated solution of large scale problems involving the interaction of electromagnetic fields with the human body. The proposed tool is based on a volume integral equation method for voxelized structures and it takes advantage of the regularity of the discretization by speeding-up the computational procedure via the Fast Fourier Transform and its inverse. Moreover, it also exploits recent advantages in the solution of Integral Equations by means of iterative preconditioned solvers. Two (parametric) Model Order Reduction schemes are then proposed where the frequency or the resistivity of the biological tissues are considered as varying parameters. The proposed tool makes analyses which otherwise would require a prohibitive computational cost affordable, such as time domain studies and uncertainty quantification in biomedical applications. The adopted formulation is focused on low frequency problems, such as the ones considered in the result section: i.e., the

evaluation of the Peripheral Nerve Stimulation due to the low-frequency magnetic field generated by the Gradient Coils of an MRI scanner during clinical examinations and the assessment of the exposure to environmental fields of live-line workers with uncertain resistivity of the biological tissues. However, the proposed approach could be also adopted for high frequency problems, like problems related to the radiofrequency field of a magnetic resonance imaging scanner, starting from other formulations suited for this kind problems [33, 49].

Acknowledgment

The results presented here were partially developed in the framework of the 17IND01 MIMAS Project. This project has received funding from the EMPIR Program, co-financed by the participating states and from the European Union's Horizon 2020 Research and Innovation Program.

References

[1] A. Arduino, U. Zanovello, J. Hand, L. Zilberti, R. Brühl, M. Chiampi, O. Bottauscio, Heating of hip joint implants in MRI: The combined effect of RF and switched-gradient fields, Magnetic Resonance in Medicine (2021) mrm.28666doi:10.1002/mrm.28666.

[2] M. Parazzini, S. Fiocchi, A. Cancelli, C. Cottone, I. Liorni, P. Ravazzani, F. Tecchio, A computational model of the electric field distribution due to regional personalized or nonpersonalized electrodes to select transcranial electric stimulation target, IEEE Transactions on Biomedical Engineering 64 (1) (2017) 184–195. doi:10.1109/TBME.2016.2553177.

[3] A. Trakic, L. Liu, H. Sanchez Lopez, L. Zilberti, F. Liu, S. Crozier, Numerical Safety Study of Currents Induced in the Patient During Rotations in the Static Field Produced by a Hybrid MRI-LINAC System, IEEE Transactions on Biomedical Engineering 61 (3) (2014) 784–793. doi:10.1109/TBME.2013.2289924.

[4] J. Lötjönen, Construction of patient-specific surface models from mr images: application to bioelectromagnetism, Computer Methods and Programs in Biomedicine 72 (2) (2003) 167–178. doi:https://doi.org/10.1016/S0169-2607(02)00125-6.

[5] I. Rubia-Rodríguez, L. Zilberti, A. Arduino, O. Bottauscio, M. Chiampi, D. Ortega, In silico assessment of collateral eddy current heating in biocompatible implants subjected to magnetic hyperthermia treatments, International Journal of Hyperthermia 38 (1) (2021) 846–861. doi:10.1080/02656736.2021.1909758.

[6] F. Fanjul-Vélez, I. Salas-García, N. Ortega-Quijano, J. L. Arce-Diego, Fdtd-based transcranial magnetic stimulation model applied to specific neurodegenerative disorders, Computer Methods

and Programs in Biomedicine 118 (1) (2015) 34–43. doi:https://doi.org/10.1016/j.cmpb.2014.10.008.

[7] S. Shahid, P. Wen, T. Ahfock, Numerical investigation of white matter anisotropic conductivity in defining current distribution under tdcs, Computer Methods and Programs in Biomedicine 109 (1) (2013) 48–64. doi:https://doi.org/10.1016/j.cmpb.2012.09.001.

[8] A. Arduino, O. Bottauscio, M. Chiampi, L. Giaccone, I. Liorni, N. Kuster, L. Zilberti, M. Zucca, Accuracy Assessment of Numerical Dosimetry for the Evaluation of Human Exposure to Electric Vehicle Inductive Charging Systems, IEEE Transactions on Electromagnetic Compatibility 62 (5) (2020) 1939–1950. doi:10.1109/TEMC.2019.2954111.

[9] O. Bottauscio, A. Arduino, D. Bavastro, D. Capra, A. Guarneri, A. A. Parizia, L. Zilberti, Exposure of Live-Line Workers to Magnetic Fields: A Dosimetric Analysis, International Journal of Environmental Research and Public Health 17 (7) (2020) 2429. doi:10.3390/ijerph17072429.

[10] K. Chan, J. Hattori, I. Laakso, A. Hirata, M. Taki, Computational dosimetry for grounded and ungrounded human models due to contact current, Physics in Medicine and Biology 58 (15) (2013) 5153–5172. doi:10.1088/0031-9155/58/15/5153.

[11] M. C. Gonzalez, A. Peratta, D. Poljak, Boundary element modeling of the realistic human body exposed to extremely-low-frequency (elf) electric fields: Computational and geometrical aspects, IEEE Transactions on Electromagnetic Compatibility 49 (1) (2007) 153–162. doi:10.1109/TEMC.2006.888167.

[12] D. Poljak, M. Cvetković, O. Bottauscio, A. Hirata, I. Laakso, E. Neufeld, S. Reboux, C. Warren, A. Giannopoulos, F. Costen, On the use of conformal models and methods in dosimetry for nonuniform field exposure, IEEE Transactions on Electromagnetic Compatibility 60 (2) (2018) 328–337. doi:10.1109/TEMC.2017.2723459.

[13] F. Tavernier, R. Scorretti, N. Burais, H. Razik, J.-Y. Gaspard, Real-time numerical dosimetry of low-frequency electromagnetic fields by using multipoles, IEEE Transactions on Magnetics 57 (6) (2021) 1–4. doi:10.1109/TMAG.2021.3065554.

[14] A. Conchin Gubernati, F. Freschi, L. Giaccone, R. Scorretti, L. Seppecher, G. Vial, Modeling of exposure to low-frequency electromagnetic fields of workers in arbitrary posture, IEEE Transactions on Magnetics 56 (2) (2020) 1–4. doi:10.1109/TMAG.2019.2949391.

[15] G. Tohumoglu, A. G. Canseven, A. Çevik, N. Seyhan, Formulation of elf magnetic fields' effects on malondialdehyde level and myeloperoxidase activity in kidney using genetic programming, Computer Methods and Programs in Biomedicine 86 (1) (2007) 1–9. doi:https://doi.org/10.1016/j.cmpb.2006.12.006.

[16] L. J. Gomez, A. C. Yücel, E. Michielssen, The icvsie: A general purpose integral equation method for bio-electromagnetic analysis, IEEE Transactions on Biomedical Engineering 65 (3) (2018) 565–574. doi:10.1109/TBME.2017.2704540.

[17] R. Hong, K. Chen, X. Hou, Q. Sun, N. Liu, Q. H. Liu, Mixed finite element method for full-wave simulation of bioelectromagnetism from dc to microwave frequencies, IEEE Transactions on Biomedical Engineering 67 (10) (2020) 2765–2772. doi:10.1109/TBME.2020.2970607.

[18] A. Arduino, O. Bottauscio, R. Brühl, M. Chiampi, L. Zilberti, *In silico* evaluation of the thermal stress induced by MRI switched gradient fields in patients with metallic hip implant, Physics in Medicine & Biology 64 (24) (2019) 245006. doi:10.1088/1361-6560/ab5428.

[19] M. Soldati, I. Laakso, Effect of electrical conductivity uncertainty in the assessment of the electric fields induced in the brain by exposure to uniform magnetic fields at 50 hz, IEEE Access 8 (2020) 222297–222309. doi:10.1109/ACCESS.2020.3043602.

[20] A. Arduino, O. Bottauscio, M. Chiampi, I. Laakso, L. Zilberti, Computational Low-Frequency Electromagnetic Dosimetry Based on Magnetic Field Measurements, IEEE Journal of Electromagnetics, RF and Microwaves in Medicine and Biology 2 (4) (2018) 302–309. doi:10.1109/JERM.2018.2869021.

[21] G. Fischer, B. Tilg, P. Wach, G. Lafer, W. Rucker, Analytical validation of the bem—application of the bem to the electrocardiographic forward and inverse problem, Computer Methods and Programs in Biomedicine 55 (2) (1998) 99–106. doi:https://doi.org/10.1016/S0169-2607(97)00060-6.

[22] W. M. Brink, R. F. Remis, A. G. Webb, A theoretical approach based on electromagnetic scattering for analysing dielectric shimming in high-field MRI: A Theoretical Approach for Analysing Dielectric Shimming, Magnetic Resonance in Medicine 75 (5) (2016) 2185–2194. doi:10.1002/mrm.25783.

[23] J. E. C. Serrallés, I. I. Giannakopoulos, B. Zhang, C. Ianniello, M. A. Cloos, A. G. Polimeridis, J. K. White, D. K. Sodickson, L. Daniel, R. Lattanzi, Noninvasive estimation of electrical properties from magnetic resonance measurements via global maxwell tomography and match regularization, IEEE Transactions on Biomedical Engineering 67 (1) (2020) 3–15. doi:10.1109/TBME.2019.2907442.

[24] I. I. Giannakopoulos, J. E. C. Serralles, L. Daniel, D. K. Sodickson, A. G. Polimeridis, J. K. White, R. Lattanzi, Magnetic-Resonance-Based Electrical Property Mapping Using Global Maxwell Tomography With an 8-Channel Head Coil at 7 Tesla: A Simulation Study, IEEE

Transactions on Biomedical Engineering 68 (1) (2021) 236–246. doi:10.1109/TBME.2020.2991399.

[25] N. Lauzeral, D. Borzacchiello, M. Kugler, D. George, Y. Rémond, A. Hostettler, F. Chinesta, A model order reduction approach to create patient-specific mechanical models of human liver in computational medicine applications, Computer Methods and Programs in Biomedicine 170 (2019) 95–106. doi:https://doi.org/10.1016/j.cmpb.2019.01.003.

[26] D. Voltolina, R. Torchio, P. Bettini, R. Specogna, P. Alotto, Optimized cycle basis in volume integral formulations for large scale eddy-current problems, Computer Physics Communications 265 (2021) 108004. doi:https://doi.org/10.1016/j.cpc.2021.108004.

[27] G. Rubinacci, S. Ventre, F. Villone, Y. Liu, A fast technique applied to the analysis of resistive wall modes with 3d conducting structures, Journal of Computational Physics 228 (5) (2009) 1562–1572. doi:https://doi.org/10.1016/j.jcp.2008.10.040.
URL https://www.sciencedirect.com/science/article/pii/S0021999108005822

[28] M. Seger, G. Fischer, R. Modre, B. Messnarz, F. Hanser, B. Tilg, Lead field computation for the electrocardiographic inverse problem—finite elements versus boundary elements, Computer Methods and Programs in Biomedicine 77 (3) (2005) 241–252. doi:https://doi.org/10.1016/j.cmpb.2004.10.005.

[29] A. Christ, W. Kainz, E. G. Hahn, K. Honegger, M. Zefferer, E. Neufeld, W. Rascher, R. Janka, W. Bautz, J. Chen, B. Kiefer, P. Schmitt, H.-P. Hollenbach, J. Shen, M. Oberle, D. Szczerba, A. Kam, J. W. Guag, N. Kuster, The Virtual Family – development of surface-based anatomical models of two adults and two children for dosimetric simulations, Physics in Medicine and Biology 55 (2) (2010) N23–N38. doi:10.1088/0031-9155/55/2/N01.

[30] M.-C. Gosselin, E. Neufeld, H. Moser, E. Huber, S. Farcito, L. Gerber, M. Jedensjö, I. Hilber, F. Di Gennaro, B. Lloyd, E. Cherubini, D. Szczerba, W. Kainz, N. Kuster, Development of a new generation of high-resolution anatomical models for medical device evaluation: the Virtual Population 3.0, Physics in Medicine and Biology 59 (18) (2014) 5287–5303. doi:10.1088/0031-9155/59/18/5287.

[31] A. C. Yucel, I. P. Georgakis, A. G. Polimeridis, H. Bağcı, J. K. White, VoxHenry: FFT-Accelerated Inductance Extraction for Voxelized Geometries, IEEE Transactions on Microwave Theory and Techniques 66 (4) (2018) 1723–1735. doi:10.1109/TMTT.2017.2785842.

[32] P. Bettini, R. Torchio, F. Lucchini, D. Voltolina, P. Alotto, Fast fourier transform-volume integral: a smart approach for the electromagnetic design of complex systems in large fusion

devices, Plasma Physics and Controlled Fusion 63 (2) (2020) 025010. doi:10.1088/1361-6587/abce8f.

[33] A. Polimeridis, J. Villena, L. Daniel, J. White, Stable fft-jvie solvers for fast analysis of highly inhomogeneous dielectric objects, Journal of Computational Physics 269 (2014) 280–296. doi:https://doi.org/10.1016/j.jcp.2014.03.026.

[34] A. Napov, Y. Notay, An algebraic multigrid method with guaranteed convergence rate, SIAM Journal on Scientific Computing 34 (2) (2012) A1079–A1109. doi:10.1137/100818509.

[35] R. Torchio, A Volume PEEC Formulation Based on the Cell Method for Electromagnetic Problems From Low to High Frequency, IEEE Transactions on Antennas and Propagation 67 (12) (2019) 7452–7465. doi:10.1109/TAP.2019.2927789.

[36] G. Fischer, B. Tilg, P. Wach, R. Modre, U. Leder, H. Nowak, Application of high-order boundary elements to the electrocardiographic inverse problem, Computer Methods and Programs in Biomedicine 58 (2) (1999) 119–131. doi:https://doi.org/10.1016/S0169-2607(98)00076-5.

[37] R. Torchio, F. Moro, G. Meunier, J.-M. Guichon, O. Chadebec, An extension of unstructured-peec method to magnetic media, IEEE Transactions on Magnetics 55 (6) (2019) 1–4. doi:10.1109/TMAG.2018.2889435.

[38] D. Voltolina, P. Bettini, P. Alotto, F. Moro, R. Torchio, High-Performance PEEC Analysis of Electromagnetic Scatterers, IEEE Transactions on Magnetics 55 (6) (2019) 1–4.

[39] D. Voltolina, R. Torchio, P. Bettini, R. Cavazzana, M. Moresco, PEEC Modeling of Planar Spiral Resonators, IEEE Transactions on Magnetics 56 (1) (2020) 1–4. doi:10.1109/TMAG.2019.2949481.

[40] V. Ardon, J. Aime, O. Chadebec, E. Clavel, J. Guichon, E. Vialardi, EMC Modeling of an Industrial Variable Speed Drive With an Adapted PEEC Method, IEEE Transactions on Magnetics 46 (8) (2010) 2892–2898. doi:10.1109/TMAG.2010.2043420.

[41] G. Antonini, D. Romano, Efficient frequency-domain analysis of peec circuits through multiscale compressed decomposition, IEEE Transactions on Electromagnetic Compatibility 56 (2) (2014) 454–465. doi:10.1109/TEMC.2013.2281393.

[42] R. Torchio, F. Lucchini, J.-L. Schanen, O. Chadebec, G. Meunier, FFT-PEEC: A Fast Tool From CAD to Power Electronics Simulations, IEEE Transactions on Power Electronics in publishing. doi:10.1109/TPEL.2021.3092431.

[43] Y. Notay, Agmg software and documentation, http://agmg.eu.

[44] G. Ninos, V. Bartzis, N. Merlemis, I. E. Sarris, Uncertainty quantification implementations in human hemodynamic flows, Computer Methods and Programs in Biomedicine 203 (2021) 106021. doi:https://doi.org/10.1016/j.cmpb.2021.106021.

[45] L. Codecasa, L. Di Rienzo, Mor-based approach to uncertainty quantification in electrokinetics with correlated random material parameters, IEEE Transactions on Magnetics 53 (6) (2017) 1–4. doi:10.1109/TMAG.2017.2666845.

[46] G. Rozza, D. B. P. Huynh, A. T. Patera, Reduced basis approximation and a posteriori error estimation for affinely parametrized elliptic coercive partial differential equations, Archives of Computational Methods in Engineering 15 (3) (2008) 229. doi:10.1007/s11831-008-9019-9.

[47] P. Benner, S. Gugercin, K. Willcox, A survey of projection-based model reduction methods for parametric dynamical systems, SIAM Review 57 (4) (2015) 483–531. doi:10.1137/130932715.

[48] M. Davids, B. Guerin, V. Klein, L. L. Wald, Optimization of MRI Gradient Coils With Explicit Peripheral Nerve Stimulation Constraints, IEEE Transactions on Medical Imaging 40 (1) (2021) 129–142. doi:10.1109/TMI.2020.3023329.

[49] E. Milshteyn, G. Guryev, A. Torrado-Carvajal, E. Adalsteinsson, J. K. White, L. L. Wald, B. Guerin, Individualized sar calculations using computer vision-based mr segmentation and a fast electromagnetic solver, Magnetic Resonance in Medicine 85 (1) (2021) 429–443. doi:https://doi.org/10.1002/mrm.28398.